Oscillation Studies on Replacement of Phase–Wound Induction Motors of a SAG Mill Drive with Permanent Magnet Synchronous Motors*

[1]E. Normanyo and [1]K. Amo-Aidoo
[1]University of Mines and Technology (UMaT), Tarkwa Ghana

Abstract

The primary objective of every industry is to optimise production at preferably lower costs. These industries make use of electric motors for their operations and the mining industry is no exception. Often is the notion to replace the Semi-Autogenous (SAG) mill drive phase-wound induction motor with an equivalent synchronous motor. This paper evaluated the correctness or otherwise of the motor replacement from the point of view of oscillations. The SAG mill drive motor was modelled and simulated using Matlab/Simulink software to ascertain the level of oscillation at start and in running mode. Both motors gave same responses at an average load of 291.385 tonnes, where they delivered same power, speed and drew the same amount of current. At maximum load of 328.571 tonnes, the Permanent Magnet Synchronous Motor (PMSM) delivered more electrical power than the PWIM, both motors exhibited a constant speed characteristic and the current drawn by the Phase-Wound Induction Motor (PWIM) was higher than that of the PMSM resulting in additional power draw of value 208.3 kW. Oscillations of the PMSM on the whole were better than those of the PWIM. The PWIM is subject to replacement in SAG mill drive systems.

Keywords: Induction Motor, Modelling, Optimise, Replacement, Simulation, Synchronous Motor

1 Introduction

A SAG mill plays a very vital role in mineral processing plants. It is responsible for the further crushing of ore meant for mineral beneficiation. In order to aid the turning effect of the SAG mill, it is mechanically coupled to an AC electric drive motor to convert electrical energy into mechanical energy. Correct selection and deployment of the electric motor enhances mill functionality.

Both the Phase-Wound Induction Motor (PWIM) and the relatively new Permanent Magnet Synchronous Motor (PMSM) are power factor dependent in operation. Compared to the PWIM, the PMSM operates at synchronous speed, constant higher power factor which is adjustable as leading, unity or lagging, lower temperature rise, it is slip speed independent, more costly for a given rating, more complicated, relatively harder to maintain, lower starting torque, greater starting current, longer starting duration and it is generally more efficient (Almeida *et al*., 2011; Gwozdziewicz and Zawilak, 2017; Isfahani and Vaez-Zadeh, 2009; Kahrisanghi *et al*., 2012). Both motors however, have slip rings and brushes. The three-phase PWIM is self-starting, speed adjustable and is known for higher overload capacity. Its power factor however, has to be kept constant at an additional cost. Both motors are preferred in fixed speed applications though a number of industrial loads require variable frequency drives. Cogging could occur especially at startup of both motors and can cause oscillations, vibrations, noise, and uneven rotation. Increasing the number of poles in a PMSM helps reduce cogging as well as the torque-ripple effect. According to Fei and Luk (2010), cogging torque is a pulsating torque occurring because of the interaction of stator teeth and rotor magnets.

A number of synchronous and induction motor comparisons for replacement have been reported in the literature. Notably, Parish *et al*. (2006) reported on replacement of a large number of induction motors with synchronous motors at the Lion Oil refinery motivated by power factor issues that result in an optimally efficient plant with low operating cost. Sethupathi and Senthilnathan (2020) compared performance of the line-start PMSM and Squirrel Cage Induction Motor (SCIM) under the influence of Customary Power Quality Indices (CPQI), Voltage Harmonic Distortion (VHD), Voltage Unbalance Factor (VUF), Long Duration Voltage Variation (LDVV) in a sugar refinery using Finite Element Analysis (FEA). They concluded that CPQI directly affects the efficiency, input power consumption, overload capacity, torque ripple and life cycle cost of both motors. Marcic *et al*. (2008) compared the Line Start Internal PMSM (LSIPMSM) with IM and concluded that the three-phase LSIPMSM exhibited sufficient line-starting performance and can therefore replace the existing IM. Sarac and Iliev (2017) compared the surface-mounted PMSM and SCIM using the finite element method. For the same power rating, the PMSM gave improved

efficiency, decreased cogging torque and improved dynamic response. They therefore concluded in favour of replacement of the asynchronous motor in wide speed range applications. Isfahani and Vaez-Zadeh (2009) investigated the Line Start PMSM (LSPMSM) on its opportunities like high efficiency, high power factor and high power density against its challenges of higher cost, extra manufacturing burden, inability to reach synchronous speed at increased load and current and torque transients waveform distortion at increased load which according to Sarac (2020), are due to the presence of higher order harmonics in the flux from the permanent magnets. They declared the LSPMSM as a great substitute to the induction motors in single speed applications. After investigating the efficiency, power factor, stator currents and rotor bar currents for steady-state performance analysis and then the rotor speed, electromagnetic torque, stator and rotor currents for dynamic performance analysis in full-load and no-load conditions using the time stepping finite element method, Kahrisanghi *et al*. (2012) declared the LSPMSMs are suitable candidates for substi-tution of induction motors in many constant-speed applications.

To the best of our knowledge, no comparative study meant for suggestion of replacement of the PWIM with the PMSM from the domain of motor oscillations especially, at start and in running mode was reported in the literature. The PWIM is noted for higher overload capacity and a better utilisation of the rotor circuit for speed and torque regulation compared to the SCIM. Also, motor oscillations are disadvantageous in typical plant environments because they give rise to vibration of machinery, dissipation of energy and a feel of discomfort to operating personnel. An extension of studies to the PWIM on motor replacement and from oscillation perspective constitute the contributions of this paper. This paper seeks to evaluate the correctness of motor replacement from the motor oscillations perspective. The rest of the paper is organised as follows: In Section 2 is presented the SAG mill, mathematical modelling of the two motors, data collection and analysis and MALAB/Simulink software based simulation, as the materials and methods used. The results and discussion are presented in Section 3 and Section 4 gives the conclusion.

2 Resources and Methods Used

2.1 Resources Used

2.1.1 The Semi-autogenous Mill

The SAG mill is a constant low speed, heavy load, high energy consuming primary grinding

equipment advantageously noted for high operation rate, large output and large crushing ratio (Wang *et al*., 2020). Fig. 1 shows a picture of the SAG mill.
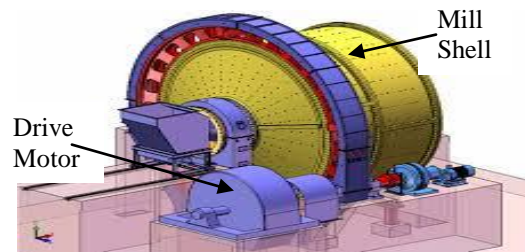
Fig. 1 A Picture of a Semi-Autogenous Mill

2.1.2 Modelling Equations of the SAG Mill Driven Motor

Generally, in the mathematical modelling of electrical machines, they are first of all described as coupled stator and rotor polyphase circuits in terms of phase variables. The next step is to transform the original stator and rotor *abc* frames of reference into a common direct-quadrature (dq0) frame in which the new variables for voltages, currents and fluxes can be viewed as 2-D space vectors. In this common frame, the inductances become constant independent of position. The dq0 transformation is a mathematical transformation that rotates the reference frame of a three-phase system in an effort to simplify the analysis of three-phase circuits. In balanced circuits, the dq0 transform reduces the three AC quantities to two DC quantities. Simplified calculations can then be carried out on these DC quantities before performing the inverse transform to recover the actual three-phase AC results (Ye *et al*., 2015).

There is also the Parks transform and the αβγ transform. The latter is the projection of the phase quantities onto a stationary two-axis reference frame while the *dq0* transform is the projection of the phase quantities onto a rotating two-axis reference frame. Transforming unto the reference frame has a number of advantages: The number of voltage equations are reduced and also the time-varying voltage equations become time-invariant equations (Krause *et al*., 2013).

Modelling Equations of the Phase-Wound Induction Motor

The asynchronous machine block in Simulink operates either as a generator or a motor, depending on the sign of the mechanical torque. If the torque is positive, it acts in the motoring mode. The electrical variables and parameters are referred to the stator, as indicated in the equations. Also, all stator and rotor quantities are in the dq0 frame. The equations, as shown are used in the modelling of the electrical system of the PWIM. The voltage

equations are given by Equation (1) (Kim, 2017; Wcislik *et al.*, 2020) and the linkage flux equations are also given by Equation (2) (Kim, 2017; Wcislik *et al.*, 2020).

$$\left.\begin{aligned}
V_{qs} &= R_s i_{qs} + \frac{d}{dt}\psi_{qs} + \omega\psi_{ds} \\
V_{ds} &= R_s i_{ds} + \frac{d}{dt}\psi_{ds} - \omega\psi_{qs} \\
V'_{qr} &= R'_r i'_{qr} + \frac{d}{dt}\psi'_{qr} + \left(\omega - \omega_r\right)\psi'_{dr} \\
V'_{dr} &= R'_r i'_{dr} + \frac{d}{dt}\psi'_{dr} - \left(\omega - \omega_r\right)\psi'_{qr} \\
T_e &= 1.5 p\left(\psi_{ds}i_{qs} - \psi_{qs}i_{ds}\right)
\end{aligned}\right\} \quad (1)$$

$$\left.\begin{aligned}
\psi_{qs} &= L_s i_{qs} + L_m i'_{qr} \\
\psi_{ds} &= L_s i_{ds} + L_m i'_{dr} \\
\psi'_{qr} &= L'_r i'_{qr} + L_m i'_{qs} \\
\psi'_{dr} &= L'_r i'_{dr} + L_m i'_{ds} \\
L_s &= L_{1s} + L_m \\
L'_r &= L'_{1r} + L_m
\end{aligned}\right\} \quad (2)$$

where, ω is reference frame angular velocity, ω_r is electrical angular velocity, L'_r is total rotor inductance, L_s is total stator inductance, R'_r and L'_r are rotor resistance and leakage inductance, respectively, V'_{qr} and i'_{qr} are q-axis rotor voltage and current, respectively, V'_{dr} and i'_{dr} are d-axis rotor voltage and current, respectively, ψ'_{qr} and ψ'_{dr} are rotor q and d-axis fluxes, respectively, ψ_{qs} and ψ_{ds} are stator q and d-axis fluxes, respectively, T_e is electromagnetic torque, p is number of pole pairs, R_s and L_{1s} are stator resistance and leakage inductance, respectively, L_m is magnetising inductance, V_{qs} and i_{qs} are q-axis stator voltage and current, respectively and V_{ds} and i_{ds} are d-axis stator voltage and current, respectively. The abc-dq0 reference frame transformations as applied to the phase-to-phase voltages of the induction machine are expressed in Equation (3) (Kim, 2017; Wcislik *et al.*, 2020).

$$\left.\begin{aligned}
\begin{bmatrix} V_{qs} \\ V_{ds} \end{bmatrix} &= \frac{1}{3}\begin{bmatrix} 2\cos\theta & \cos\theta + \sqrt{3}\sin\theta \\ 2\sin\theta & \sin\theta - \sqrt{3}\cos\theta \end{bmatrix}\begin{bmatrix} V_{abs} \\ V_{bcs} \end{bmatrix} \\
\begin{bmatrix} V'_{qr} \\ V'_{dr} \end{bmatrix} &= \frac{1}{3}\begin{bmatrix} 2\cos\beta & \cos\beta + \sqrt{3}\sin\beta \\ 2\sin\beta & \sin\beta - \sqrt{3}\cos\beta \end{bmatrix}\begin{bmatrix} V'_{abr} \\ V'_{bcr} \end{bmatrix}
\end{aligned}\right\} \quad (3)$$

where, θ is angular position of the reference frame and $\beta = \theta - \theta_r$ is difference between the position of

the reference frame and the electrical position of the rotor.

The dq0-to-abc reference frame transformations applied to the phase currents of the induction machine are given by Equation (4) (Kim, 2017; Wcislik *et al.*, 2020) and finally, it is assumed that saturation effects are inexistent.

$$\left.\begin{aligned}
\begin{bmatrix} i_{as} \\ i_{bs} \end{bmatrix} &= \begin{bmatrix} \cos\theta & \sin\theta \\ \dfrac{-\cos\theta + \sqrt{3}\sin\theta}{2} & \dfrac{-\sqrt{3}\cos\theta - \sin\theta}{2} \end{bmatrix}\begin{bmatrix} i_{qs} \\ i_{ds} \end{bmatrix} \\
\begin{bmatrix} i'_{ar} \\ i'_{br} \end{bmatrix} &= \begin{bmatrix} \cos\beta & \sin\beta \\ \dfrac{-\cos\beta + \sqrt{3}\sin\beta}{2} & \dfrac{-\sqrt{3}\cos\beta - \sin\beta}{2} \end{bmatrix}\begin{bmatrix} i'_{qr} \\ i'_{dr} \end{bmatrix} \\
i_{cs} &= -i_{as} - i_{bs} \\
i'_{cr} &= -i'_{ar} - i'_{br}.
\end{aligned}\right\} \quad (4)$$

Modelling equations of the permanent magnet synchronous motor

In synchronous machine studies, the two-axis equivalent with two or three damping windings are usually assumed at the proper structures. In developing the basic equations of a synchronous machine, the following assumptions are made (Barakat *et al*, 2010): Stator windings are symmetrical and have a perfect sinusoidal distribution along the air gap, permeation of the magnetic paths on the rotor is independent of the rotor positions and lastly, saturation and hysteresis effects are inexistent. Saliency of the rotor and the field excitation make the synchronous machine asymmetrical, and as such the corresponding dq model uses the rotor coordinates as reference frame. The model takes into account the dynamics of the stator, field and damper windings. The rotor reference frame is adapted and all rotor parameters and electrical quantities are viewed from the stator.

Park's transformation is applied to map the synchronous machine equations to the rotating reference frame, with respect to the electrical angle. Park's transformation is defined by Equation (5) (Bassey and Ogbuka, 2015; Kim, 2017).

$$P_s = \frac{2}{3}\begin{bmatrix} \cos\theta_e & \cos\left(\theta_e - \dfrac{2\pi}{3}\right) & \cos\left(\theta_e + \dfrac{2\pi}{3}\right) \\ -\sin\theta_e & -\sin\left(\theta_e - \dfrac{2\pi}{3}\right) & -\sin\left(\theta_e - \dfrac{2\pi}{3}\right) \\ \dfrac{1}{2} & \dfrac{1}{2} & \dfrac{1}{2} \end{bmatrix} \quad (5)$$

where, θ_e is electrical angle. The transformation is used to define the per-unit motor equations, still in the dq0 transformation. The stator voltage

equations are given by Equation (6) (Bassey and Ogbuka, 2015; Kim, 2017).

$$
\left.\begin{aligned}
e_d &= \frac{d}{dt}\frac{\psi_d}{\omega_{base}} - \psi_q \omega_r - R_a i_d \\
e_q &= \frac{d}{dt}\frac{\psi_q}{\omega_{base}} + \psi_d \omega_r - R_a i_q \\
e_0 &= \frac{d}{dt}\frac{\psi_0}{\omega_{base}} - R_a i_0
\end{aligned}\right\} \tag{6}
$$

where, e_d, e_q and e_0 are d-axis, q-axis and zero-sequence stator voltages, respectively. They are defined by Equation (7) (Bassey and Ogbuka, 2015; Kim, 2017).

$$
\begin{bmatrix} e_d \\ e_q \\ e_0 \end{bmatrix} = P_s \begin{bmatrix} V_a \\ V_b \\ V_c \end{bmatrix} \tag{7}
$$

where, V_a, V_b and V_c are measured port to neutral stator voltages of the respective phases, ω_{base} is per-unit base electrical speed, ψ_d, ψ_q and ψ_0 are d-axis, q-axis and zero-sequence stator flux linkages, respectively, ω_r is per-unit rotor rotational speed, R_a is stator resistance and i_d, i_q and i_0 are d-axis, q-axis and zero sequence stator currents. The zero sequence stator currents are defined by Equation (8) (Bassey and Ogbuka, 2015; Kim, 2017).

$$
\begin{bmatrix} i_d \\ i_q \\ i_0 \end{bmatrix} = P_s \begin{bmatrix} i_a \\ i_b \\ i_c \end{bmatrix} \tag{8}
$$

where, i_a, i_b and i_c are stator currents of the respective phases. The rotor voltage equations are defined by Equation (9) (Bassey and Ogbuka, 2015; Kim, 2017).

$$
\left.\begin{aligned}
e_{fd} &= \frac{d}{dt}\frac{\psi_{fd}}{\omega_{base}} + R_{fd} i_{fd} \\
e_{1d} &= \frac{d}{dt}\frac{\psi_{1d}}{\omega_{base}} + R_{1d} i_{1d} = 0 \\
e_{1q} &= \frac{d}{dt}\frac{\psi_{1q}}{\omega_{base}} + R_{1q} i_{1q} = 0
\end{aligned}\right\} \tag{9}
$$

where, e_{fd} is field voltage, e_{1d} and e_{1q} are voltages across the d-axis damper winding 1 and q-axis damper winding 1, respectively. They are equal to 0, ψ_{fd}, ψ_{1d} and ψ_{1q} are magnetic fluxes linking the field circuit, d-axis damper winding 1 and q-axis damper winding 1, respectively, R_{fd},

R_{1d} and R_{1q} are resistances of the rotor field circuit, d-axis damper winding 1, respectively, and q-axis damper winding 1 and i_{fd}, i_{1d} and i_{1q} are currents flowing in the field circuit, d-axis damper winding 1, and q-axis damper winding 1, respectively . The stator flux linkage equations are defined by Equation (10) (Bassey and Ogbuka, 2015; Kim, 2017).

$$
\left.\begin{aligned}
\psi_d &= -\left(L_{ad} + L_i\right) i_d + L_{ad} i_{fd} + L_{ad} i_{1d} \\
\psi_q &= -\left(L_{aq} + L_i\right) i_d + L_{aq} i_{1d} \\
\psi_0 &= -L_0 i_0
\end{aligned}\right\} \tag{10}
$$

where, L_0 is stator leakage inductance, L_{ad} and L_{aq} are mutual inductances of the d-axis and q-axis, respectively. The rotor flux linkage equations are defined by Equation (11) (Bassey and Ogbuka, 2015; Kim, 2017).

$$
\left.\begin{aligned}
\psi_{fd} &= L_{ffd} i_{fd} + L_{f1d} i_{1d} - L_{ad} i_d \\
\psi_{1d} &= L_{f1d} i_{fd} + L_{11d} i_{1d} - L_{ad} i_d \\
\psi_{fd} &= L_{11q} i_{1q} - L_{aq} i_q
\end{aligned}\right\} \tag{11}
$$

where, L_{ffd}, L_{11d} and L_{11q} are self-inductances of the rotor field circuit, d-axis damper winding 1, and q-axis damper winding 1, respectively and L_{f1d} is rotor field circuit and d-axis damper winding 1 mutual inductance. These parameters are defined by Equation (12) (Bassey and Ogbuka, 2015; Kim, 2017).

$$
\left.\begin{aligned}
L_{ffd} &= L_{ad} + L_{fd} \\
L_{f1d} &= L_{ffd} - L_{fd} \\
L_{11d} &= L_{f1d} + L_{1d} \\
L_{11q} &= L_{aq} - L_{1q}
\end{aligned}\right\} \tag{12}
$$

These equations assume that the per-unit mutual inductance $L_{12q} = L_{aq}$, i.e., the stator and rotor currents in the q-axis all link a single mutual flux represented by L_{aq}. The rotor torque is given by Equation (13) (Bassey and Ogbuka, 2015; Kim, 2017).

$$
T_e = \psi_d i_q - \psi_q i_d \tag{13}
$$

2.1.3 Data Collection and Analysis

Data on a SAG mill was collected from a gold mine in the Tarkwa Nsuaem Municipality in the Western Region of Ghana. For the simulations, data on the inputs of the mill motor taken on a daily basis (on the average) and motor data were utilised. These data are presented in Table 1 and Table 2, respectively.

15

Table 1 SAG Mill Operational Data

Time	Current (A)	Power (kW)	Voltage (V)	Feed Rate (Tonnes/hr.)	Weight (kg)	Density (kg/m³)
3:46 am	136.239	2271.440	11299.145	347.863	289.011	1.6788
4:07 am	117.094	2385.329	11295.482	327.228	281.978	1.6810
4:29 am	131.795	2454.092	11180.708	387.302	305.055	1.6954
4:51 am	141.197	2380.250	11228.327	400.000	285.495	1.7154
5:13 am	140.855	2279.840	11310.134	412.210	282.637	1.6981
5:35 am	130.598	2461.418	10907.204	402.320	286.593	1.7054
5:56 am	138.803	2302.696	10843.712	424.420	283.956	1.7237
6:18 am	139.658	2281.793	10852.259	410.501	284.615	1.7192
6:40 am	128.547	2364.524	10753.358	398.168	283.516	1.7225
7:02 am	132.650	2302.989	10897.436	403.297	283.956	1.7195
7:24 am	125.299	2352.901	11017.094	397.192	284.176	1.7030
7:46 am	131.624	2421.762	11302.808	395.116	287.033	1.7073
8:07 am	144.615	2521.000	11582.418	404.151	291.648	1.7218
8:29 am	115.043	2496.679	11633.700	382.418	291.209	1.7074
8:51 am	139.316	2347.725	11642.247	412.210	283.956	1.7036
9:13 am	138.120	2625.513	11708.181	395.482	291.648	1.6989
9:35 am	130.940	2589.861	11227.106	385.470	296.484	1.7020
9:56 am	133.162	2445.790	11345.543	391.819	287.912	1.7238
10:18 am	134.017	2442.958	11277.167	402.930	289.451	1.7261
10:40 am	122.393	2363.157	11692.308	404.151	286.154	1.7353
11:02 am	127.179	2328.580	11686.203	395.604	283.297	1.7238
11:24 am	137.436	2493.065	11730.159	381.685	277.582	1.7183
11:46 am	117.607	2379.762	11721.612	403.053	287.253	1.7150
12:07 pm	140.684	2496.874	11452.991	394.628	291.868	1.7153
12:29 pm	147.863	2545.810	11133.089	421.978	293.846	1.6773
12:51 pm	145.812	2420.785	11039.072	405.250	292.967	1.7237
1:13 pm	116.410	2431.432	11041.514	399.023	290.769	1.7304
1:35 pm	120.000	2509.181	11224.664	395.116	293.187	1.7256
1:56 pm	115.043	2635.182	11633.700	392.674	294.505	1.7331

Table 2 Phase-Wound Motor Nameplate Data

Motor Parameter	Value	Unit
Output power	3750	kW
Speed	600	rev/min
Supply voltage	11000	V
Number of phases	3	
Frequency	50	Hz
Power factor	0.9	
Excitation current	272	A
Excitation voltage	119	V
Input current	226	A
Input power	4300	kVA
Input connection	Star	

The data are mainly based on the current, power and voltage drawn and the weight of the SAG mill over a 12 hour period of operation. The minimum average and maximum values of each of the parameters are derived from the data. In terms of the current drawn, the minimum, average and maximum values over the stated period are 91.4533 A, 131.042 A and 169.402 A, respectively. In terms of the voltage, the recorded values are 10476.190

V, 11137.235 V and 11730.159 V as the minimum, average and maximum voltages, respectively. The weight of the mill is also stated in the data. The average weight of the SAG mill recorded was 291.385 tonnes whilst the maximum was 328.571 tonnes, with corresponding feed rates of 376.687 tonnes/hr and 424.420 tonnes/hr, respectively. Therefore, the corresponding power drawn at the stated maximum load is 3097.187 kW whilst that of the average weight is found by interpolation to be 2708.279 kW. These changes in power draw are used for the simulations. For the general motor data, the synchronous motor is a 3.75 MW, 10-pole, 50 Hz motor and the induction motor is also a 10-pole, 50 Hz, 3.75 MW motor of the phase wound rotor type.

2.2 Methods Used

Motor simulations were conducted based on the modelling equations and the field data. Two scenarios were considered in the simulations for each mill driven motor: Scenario 1 gives simulation under normal operating conditions with an average load of 291.385 tonnes having a corresponding

power draw of 2708.279 kW, while Scenario 2 refers to the situation of maximum load of 328.571 tonnes with a corresponding power draw of 3097.187 kW. The SAG mill load driven by motor contains in addition to the weight of empty mill, steel balls, water and dry ore, and these together constitute the weight of the SAG mill.

In this mode, the mechanical power at the machine shaft input is a negative function, which can be varied using the step input block. For the simulations, the two AC motors were deployed one after the other for configuration: First was the PWIM and later the PMSM. Fig. 2 shows the simulink model of the AC motor representing the PWIM or the PMSM. For both motors, the stator current, rotor speed and output electrical power signals were scoped for analysis for possible oscillations.

3 Results and Discussion

3.1 Simulation Results

Fig. 3, Fig. 4, Fig. 5 and Fig. 6 show the respective responses of the two motors for average and maximum load.

3.2 Discussion of Simulation Results

For the average load, the PWIM stator current, i_s, started with ripples (see Fig. 3) which decrease gradually and stabilised to about 23 A after 2 secs. That of the PMSM (see Fig. 5) started off smoothly for 0.5 sec and then became unstable evidenced by the high frequency oscillations for 2 secs, after which it also stabilised to 23 A. The instability exhibited by PMSM at maximum load could be due to the presence of higher order current and torque harmonics caused by the permanent magnet generated magnetic flux density. The speed, N, also was unstable for 2 secs, but stabilised at the rated 600 rpm. In the case of the PWIM, the instability occured also for 2 secs after which the speed settled at 600 rpm. The output electrical power, P_{eo}, responded to the load and oscillated for 2 secs before stabilising at 2437.5 kW. For the maximum load, it can be seen from Fig. 6 that the stator current, i_s, of the PMSM oscillated at high frequencies for 0.5 sec, after which the frequencies decreased and finally settled after 2.5 secs. With the PWIM, from Fig. 4, the oscillations began at a lesser frequency and settled after 2 secs. It drew more current as compared to the PMSM. The speed of both motors settled at 600 rpm after 2 sec. The PMSM output electrical power delivered settled at 3575 kW as against 3166.7 kW for PWIM after the 2 secs.

Summarily, for an average load, the responses of both motors are the same, delivering same power, speed and drawing the same amount of current. For the maximum load, based on the responses, the PMSM delivered more electrical power than the PWIM, both motors exhibited a constant speed characteristic and the current drawn by the PWIM was higher than that of the PMSM.
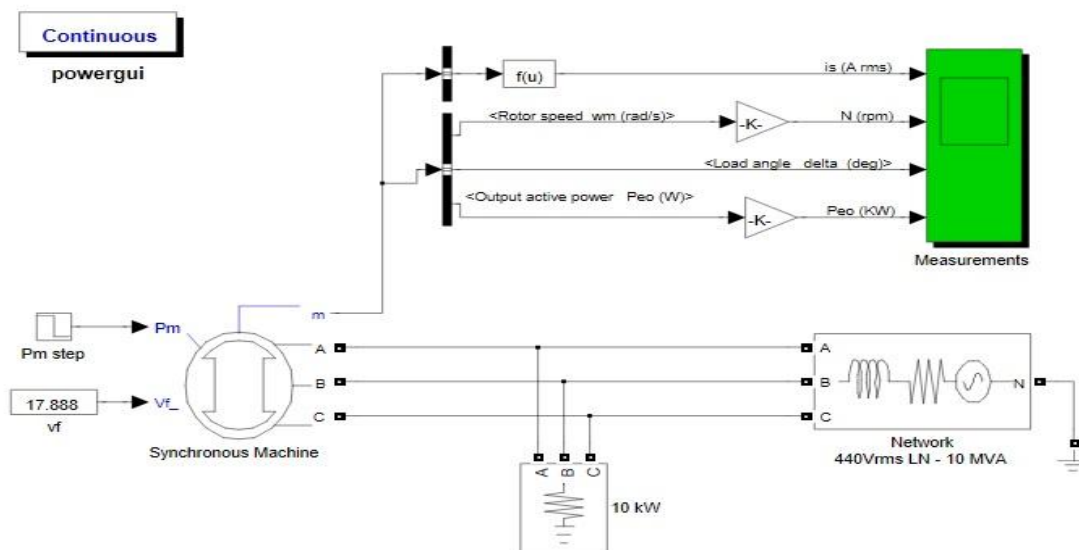
Fig. 2 Simulink Model of the AC Motor
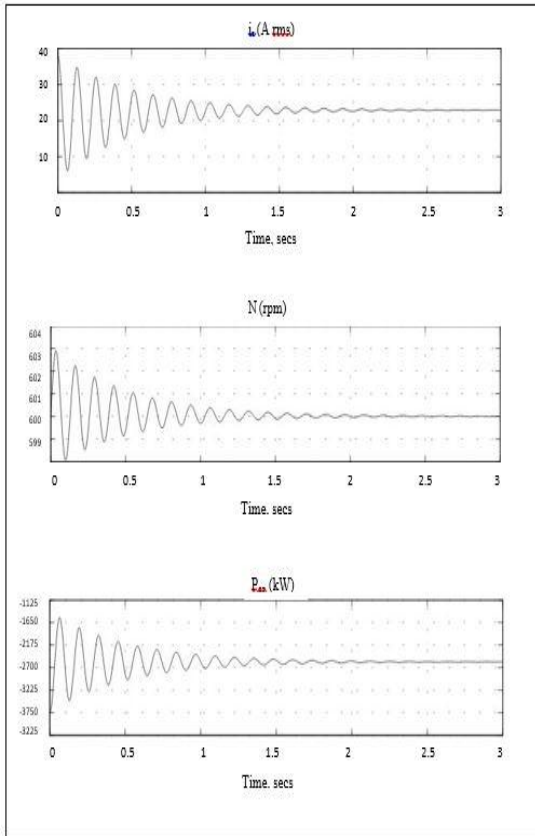
Fig. 3 Responses of the Induction Motor to the Average Load of 291.385 Tonnes
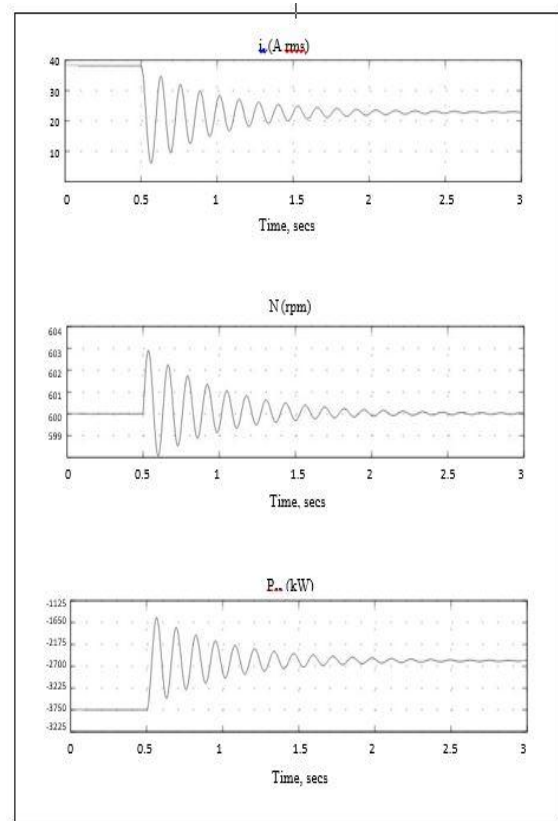
Fig. 5 Responses of the Permanent Magnet Synchronous Motor to the Average Load of 291.385 Tonnes
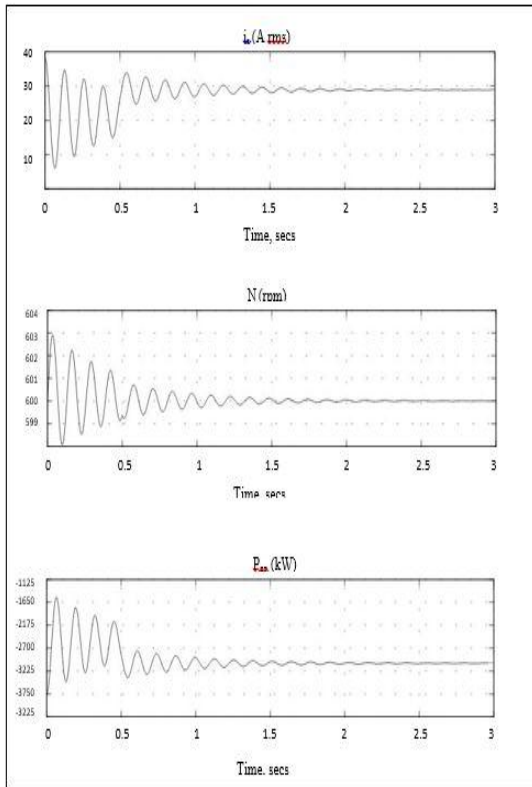
Fig. 4 Responses of the Induction Motor to the Maximum Load of 328.571 Tonnes
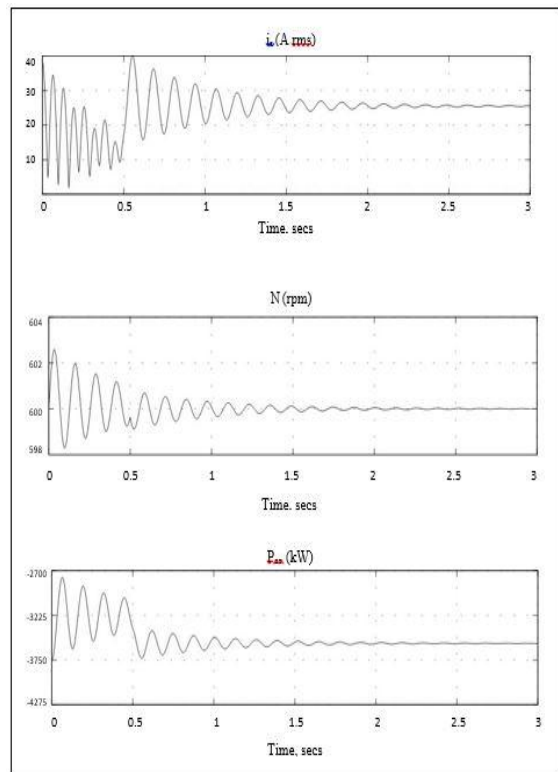
Fig. 6 Responses of the Permanent Magnet Synchronous Motor to the Maximum Load of 328.571 Tonnes

4 Conclusion

In conclusion, it is feasible to replace the PWIM with the PMSM. In particular, for maximum load the PMSM is more preferable to the PWIM. Since the SAG mill is usually operated at around maximum load, it will be more advantageous in terms of output electrical power, speed, current drawn and stability to consider the PMSM for deployment as the prime mover in SAG mills. Future work however, could look into the mechanical reasons why replacement could be necessary. This investigation centered on the electrical aspect, considering only the electric motors and the loads in question.

References

Barakat, A., Tnani, S., Champenois, G. and Mouni, E. (2010), "Analysis of Synchronous Machine Modelling for Simulation and Industrial Applications", *Simulation Modelling Practice and Theory*, Vol. 18, No. 9, pp. 1382-1396.

Bassey, O. and Ogbuka, C. U. (2015), "Modelling and Simulation of the Startup Performance of Grid-connected Permanent Magnet Synchronous Motor (PMSM)", *International Conference on Electric Power Engineering (ICEPENG 2015),* Department of Electrical Engineering, University of Nigeria, Nsukka, Nigeria, pp. 69-74.

De Almeida, A. T., Ferreira, F. J. T. E. and Fong, J. A. C. (2011), "Standards for Efficiency of Electric Motors, Permanent Magnet Synchronous Motor Technology", *IEEE Industry Applications Magazine*, Vol. 17, No. 1, pp.12-19.

Fei, W. and Luk, P. C. K. (2010), "A New Technique of Cogging Torque Suppression in Direct-drive Permanent Magnet Brushless Machine", *IEEE Transactions on Industry Applications*, Vol. 46, No. 4. pp. 1332-1340.

Gwozdziewicz M. and Zawilak, J. (2017), "Induced Pole Permanent Magnet Synchronous Motor," *2017 International Symposium on Electrical Machines (SME)*, Naleczow,· Lubelskie, Poland, pp. 1-4, doi: 10.1109/ISEM.2017.799-3543.

Isfahani, A. H. and Vaez-Zadeh, S. (2009), "Line Start Permanent Magnet Synchronous Motors: Challenges and Opportunities", *Energy*, Vol. 34, pp. 1755–1763.

Kahrisangi, M. G., Isfahani, A. H., Vaez-Zadeh, S. and Sebdani, M. R. (2012), "Line-start Permanent Magnet Synchronous Motors versus Induction Motors: A Comparative Study", *Frontiers of Electrical and Electronic Engineering*, Vol. 7, No. 4, pp. 459–466.

Kim, S_H. (2017), "Modelling of Alternating Current Motors and Reference Frame Theory', Chapter 4 in: *Electric Motor Control*, 1st edition, Elsevier Science, Netherlands, 438 pp.

Krause, P., Wasynczuk, O., Sudhoff, S. and Pekarek, S. (2013), *Analysis of Electric Machinery and Drive Systems*, 3rd edition, John Wiley and Sons, Inc., Hoboken, New Jersey, USA, 659 pp.

Marcic, T., Stumberger, B., Stumberger G., Hadziselimovic, M., Virtic, P. and Dolinar, D. (2008), "Line-Starting Three- and Single-Phase Interior Permanent Magnet Synchronous Motors—Direct Comparison to Induction Motors", *IEEE Transactions on Magnetics*, Vol. 44, No. 11, pp. 4413-4416.

Parrish, J., Moll, S. and Schaefer, R. C. (2006), "Synchronous versus Induction Motors: Plant Efficiency Benefits Resulting from the Use of Synchronous Motors", *IEEE Industry Applications Magazine*, Vol. 12, No. 2, pp. 61-70.

Šarac, V. (2020), "Line-start Synchronous Motor: A Viable Alternative to Asynchronous Mo-tor", *Facta Universitatis Series: Automatic Control and Robotics*, Vol. 19, No 1, pp. 39 – 58. https://doi.org/10.22190/FUACR2001039S

Šarac, V. and Iliev, D. (2017), "Synchronous Motor of Permanent Magnet Compared to Asynchronous Induction Motor", *Electrotehnica, Electronica, Automatica*, Vol. 65, No. 7, pp. 51-58.

Sethupathi, P. and Senthilnathan, N. (2020), "Comparative Analysis of Line-start Permanent Magnet Synchronous Motor and Squirrel Cage Induction Motor under Customary Power Quality Indices", *Electrical Engineering*, pp. 1-11, *https://doi.org/10. 1007/s00202-020-00955-2.* Accessed: July 1, 2020.

Wang X., Yi, J., Zhou, Z. and Yang, C. (2020), "Optimal Speed Control for a Semi-Autogenous Mill based on Discrete Element Method", *Processes*, Vol. 8, pp. 1-17, doi:10. 3390/pr8020233.

Wcislik, M., Suchenia, K. and Cyganik, A. (2017), "Vectorised Mathematical Model of a Slip-Ring Induction Motor", *Energies 2020*, 13, 4015, pp. 1-20. doi:10.3390/en13154015.

Ye, H., Tang, Y. and Xia, Y. (2015), "DQ-domain Modelling for Multi-scale Transients in a Synchronous Machine", *Proceedings of the 5th International Conference on Electric Utility Deregulation and Restructuring and Power Technologies*, Changsha, China, pp. 285-289.

Authors

E. Normanyo is a Senior Lecturer in the Electrical and Electronic Engi- neering Department at the University of Mines and Technology, Tarkwa, Ghana. He holds MSc degree in Electromechanical Engineering from the Kharkov State University, Ukraine. He is a member of the Ghana Institution of Engineers. His research interests include industrial automation, industrial energy management,

instrumentation systems, control engineering, artificial intelligence, automated electric drives and mechatronics.

K. Amo Aidoo is currently a Power Systems Instrumentation Engineer at Electricity Company of Ghana, Kumasi, Ghana. He holds BSc degree in Electrical and Electronic Engineering from the University of Mines and Technology (UMaT), Tarkwa. His research interests include instrumentation, industrial automation and energy management.